

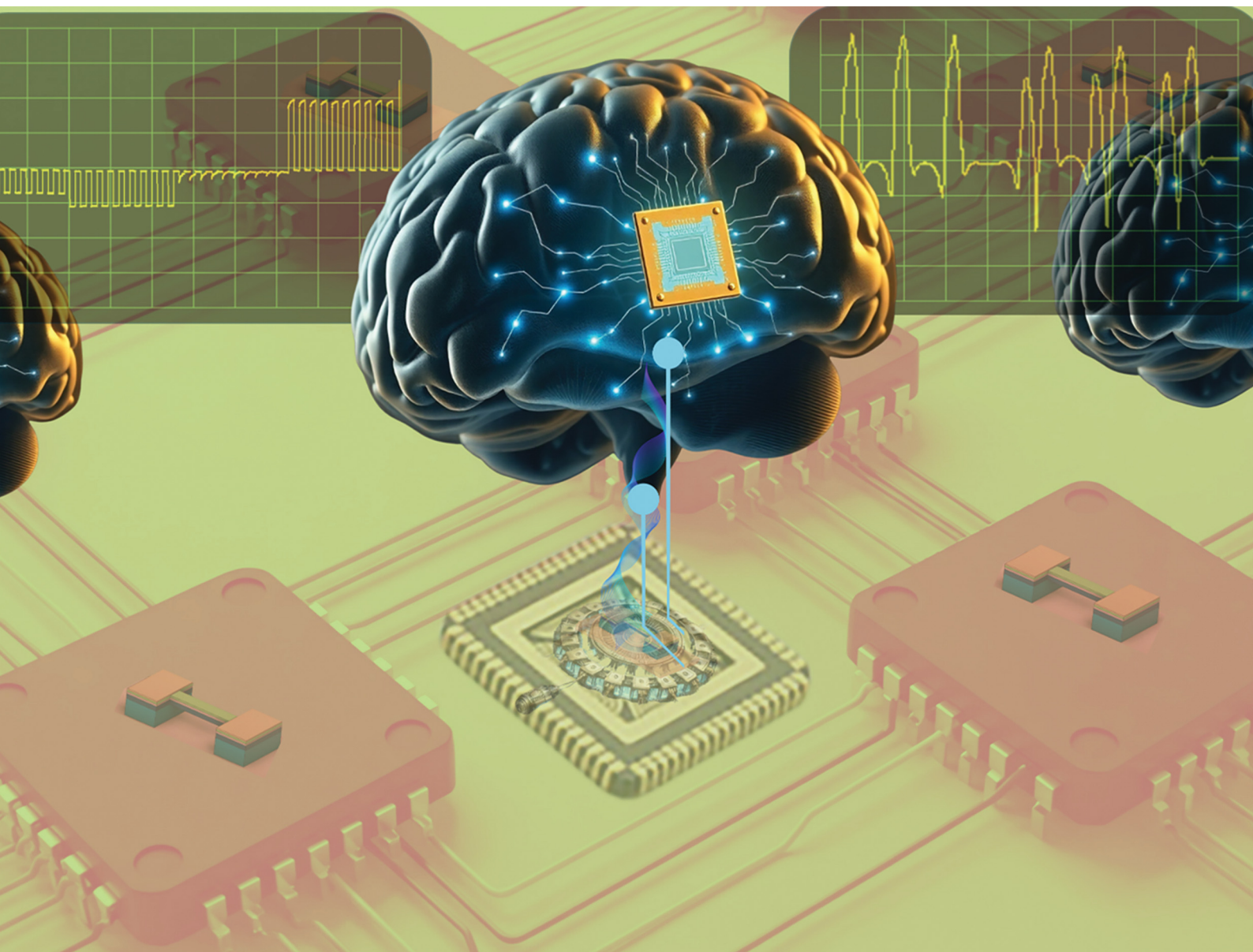
# Nanoscale Horizons

The home for rapid reports of exceptional significance in nanoscience and nanotechnology

[rsc.li/nanoscale-horizons](https://rsc.li/nanoscale-horizons)

Volume 10  
Number 3  
March 2025  
Pages 413–650

10  
YEARS  
ANNIVERSARY



ISSN 2055-6756

**COMMUNICATION**

Ankur Goswami *et al.*

Electric field-assisted resonance frequency tuning in free standing nanomechanical devices for application in multistate switching using a phase change material



Cite this: *Nanoscale Horiz.*, 2025, 10, 549

Received 12th September 2024,  
Accepted 21st October 2024

DOI: 10.1039/d4nh00463a

[rsc.li/nanoscale-horizons](https://rsc.li/nanoscale-horizons)

# Electric field-assisted resonance frequency tuning in free standing nanomechanical devices for application in multistate switching using a phase change material†

Durgesh Banswar,<sup>†a</sup> Jay Krishna Anand,<sup>†a</sup> Syed A. Bukhari,<sup>cd</sup> Sonika Singh,<sup>ib</sup> Rahul Prajesh,<sup>e</sup> Hemant Kumar,<sup>f</sup> S. K. Makineni<sup>f</sup> and Ankur Goswami<sup>ib\*ab</sup>

VO<sub>2</sub> possesses a unique property of solid-state phase transition near room temperature wherein it transforms from monoclinic (M1) to tetragonal phase (R) that alters its physical properties, such as resistivity, mechanical modulus, and lattice strain, at an ultrafast time scale known as MIT. Such a phenomenon offers a distinct advantage to use VO<sub>2</sub> in switching applications using heat flux as a stimulus. However, such alteration in properties can also be triggered under an electric field (*E*), which is known as E-MIT. A nanomechanical resonator coated with VO<sub>2</sub> recently received traction where the resonance behavior can be modulated by taking advantage of its phase transition. Herein, we demonstrate that by fabricating a microstring of 400 μm (*L*) × 5 μm (*W*) × 240 nm (*t*) of suspended SiN<sub>x</sub> coated with VO<sub>2</sub>, the frequency (*f<sub>r</sub>*) of the resonator can be modulated by applying an electric field. We show that at room temperature, the *f<sub>r</sub>* of the microstring can be either reduced (by 0.5% at 15 V mm<sup>−1</sup>) or enhanced (by 2.2% at 25 V mm<sup>−1</sup>) or can be varied in a cycle under *E*-field. Using theoretical models, we establish the simulated results and explain the processes behind it, which demonstrate excellent mechanical tuning properties of the VO<sub>2</sub>-based microstring resonator, making it an attractive and alternative option for highly efficient MEMS-based switches and neuromorphic devices.

## New concepts

This work reports a route to unveil the multi-stable switching state of *E*-field induced mechanical modulation of VO<sub>2</sub> coated nanomechanical microstring resonator. The microstring resonator vibrating at its resonating frequency (*f<sub>r</sub>*) can be altered by applying varied *E*-field. We observed that on the application of periodic square pulses of *E*-field, the nanomechanical device showed periodic variation in its resonance frequency. However, this periodic vibration can be excited to multiple stable states upon varying the amplitude of periodic *E*-field. The observation of such phenomena in terms of mechanical frequency by modulation of *E*-field is unique and finds direct application in switching devices illustrated in this work. This multiple stable states of vibrations at room temperature is mainly due to the incorporation of TiO<sub>2</sub> as an interfacial beneath VO<sub>2</sub> that brings down the metal-insulator transition temperature of VO<sub>2</sub> from ideal 67 °C to room temperature (around 30–35 °C). A direct observation of this lowered transition temperature was revealed by a few experimental measurements, such as observing variation in resistance as a function of temperature, change in resonance frequency with the temperature and temperature dependent Raman spectroscopic measurements.

## 1. Introduction

Nanomechanical resonators have been a great area of interest in the scientific community because of their extensive diversity of applications, including gas sensing and olfactory detection,<sup>1–3</sup> photon and IR detection, phase transition studies, energy harvesting,<sup>4</sup> actuation,<sup>5,6</sup> mechanical property determination,<sup>7</sup> molecular manipulation,<sup>8</sup> and information processing.<sup>9–11</sup> Nano-mechanical resonators have received significant attention recently after the incorporation of phase change materials into this technology.<sup>12</sup> Phase change materials possess unique advantages in creating stress, strain and force gradient due to the alteration of their intrinsic properties (like elastic modulus, thermal expansion coefficient, and magnetic properties) owing to the external stimuli (electric field, magnetic field, thermal, and optical), which is the basis of actuating devices.<sup>13–15</sup> In order to address this purpose, transition metal oxides (TMOs) have been exploited extensively in the recent past where phase transitions arise from electronic correlation, lattice distortion and magnetic ordering, which give

<sup>a</sup> Department of Materials Science and Engineering, Indian Institute of Technology, Delhi, Hauz Khas, New Delhi 110016, India. E-mail: [agoswami@mse.iitd.ac.in](mailto:agoswami@mse.iitd.ac.in)

<sup>b</sup> School of Interdisciplinary Research (SIRe), Indian Institute of Technology, Delhi, Hauz Khas, New Delhi 110016, India

<sup>c</sup> Department of Chemical and Materials Engineering, University of Alberta, Edmonton, AB, T6G 1H9, Canada

<sup>d</sup> Texas Instruments, Dallas, TX 75243, USA

<sup>e</sup> Semiconductor Sensors and Microsystems Group, CSIR-CEERI, Pilani 333031, India

<sup>f</sup> Department of Materials Engineering, Indian Institute of Science, Bengaluru 560012, India

† Electronic supplementary information (ESI) available. See DOI: <https://doi.org/10.1039/d4nh00463a>

‡ Durgesh Banswar and Jay Krishna Anand contribute equally to this paper.

rise to the nonlinear change in various physical properties.<sup>16,17</sup> Vanadium dioxide ( $\text{VO}_2$ ) is one of the candidates in the family of TMOs that shows such nonlinear variations in its physical properties at 68 °C (ideally) due to the structural phase transition (SPT) from monoclinic (M1) to tetragonal (R) phase like martensite. In its monoclinic phase,  $\text{VO}_2$  is electrically insulating or semiconducting in nature and exhibits conducting nature in the tetragonal phase. This unique behavior of  $\text{VO}_2$  around room temperature (around 68 °C) offers extra advantages over other materials that exhibit similar nature either at a very high temperature (e.g.:  $\text{NbO}_2$  at 800 °C) or at a very low temperature (e.g.:  $\text{Fe}_3\text{O}_4$  at −154 °C,  $\text{V}_2\text{O}_3$  at −123 °C). Furthermore, such a transition is believed to occur at a very fast rate (ultrafast scale). However, it is difficult to track such fast transition as it is limited by various constraints, such as heat dissipation rate of the material (thermal conductivity and heat capacity of the material), geometry of the device and measurement difficulties, such as data acquisition rate of the measuring instrument. Nevertheless, such fast transition is an encouraging factor to explore  $\text{VO}_2$  for different applications requiring quick response time when subjected to external stimuli. This transition is reversible in nature and occurs because of its change in crystal symmetry due to the transformation from monoclinic (M1) insulating phase (space group  $P2_1/c$ ) to rutile (R) metallic phase (space group  $P4_2/mnm$ ).<sup>18</sup> More precisely, the dimerization of alternating V atoms, which results in two different V–V bond lengths and tilting of these dimers with respect to the *c*-axis causes the transition.<sup>19</sup> Although the mechanism of the transition still remains elusive, with two possible scenarios: a lattice distortion driven (Peierls-like) or an electron correlation driven (Mott-like),<sup>20</sup> recently it has been proposed that the transition happens due to the strong interaction of electrons and phonons and hence it is described as “Mott-assisted Peierls” mechanism.<sup>18</sup>

Despite the puzzling physics of  $\text{VO}_2$ , it has been widely explored in a variety of technological applications such as thermal,<sup>21</sup> optical,<sup>22–24</sup> electronic<sup>25</sup> and thermoelastic switches,<sup>26</sup> smart windows,<sup>27</sup> microbolometer,<sup>28</sup> nonvolatile and programmable memory,<sup>29,30</sup> memristors,<sup>31</sup> and actuators.<sup>32</sup> Most of these applications are explored by exploiting the electronic properties of  $\text{VO}_2$ . For instance, variation of its electrical conductance by the thermal stimulus is key for smart windows,<sup>27</sup> microbolometer<sup>33</sup> and thermal switches applications.<sup>34</sup> On the other hand,  $\text{VO}_2$  also changes its electrical conductance isothermally under a critical electric field ( $E_c$ ), which is known to be electric field-assisted metal–insulator transition (E-MIT).<sup>19,35,36</sup> This property has been widely explored in nonvolatile memory, memristors and neuromorphic devices.<sup>37</sup> Although there are numerous reports on  $\text{VO}_2$ -based devices taking advantage of the electrical conductance change, however, there are few reports on variation of mechanical responses when it undergoes a thermal cycle.<sup>38,39</sup> Rúa *et al.* were the first to observe this phenomenon by measuring the bending of  $\text{VO}_2$  microcantilever,<sup>40</sup> whereas McGee *et al.* and Bukheri *et al.* showed similar behavior by measuring frequency change with the function of temperature and optical illumination.<sup>38,40–42</sup> Recently, such modulation of mechanical responses was also observed by photothermal actuation by Wang *et al.*<sup>43</sup> However, there is no such report where

mechanical modulation can be controlled isothermally by manipulating DC electric field, taking the advantage of E-MIT property of the  $\text{VO}_2$ . In this work, we report modulation of mechanical frequency of a suspended  $\text{VO}_2$ -coated microstring using DC electric-field. The suspended  $\text{VO}_2$  microstring was allowed to vibrate using a piezoelectric vibrator. We show that the resonance frequency of the microstring can be reduced from its original value by applying the electric field lower than the critical  $E_c$  whereas it can be enhanced by applying higher than  $E_c$ . The theoretical studies using the finite element method (FEM) employing COMSOL were performed to verify the E-MIT behavior of the  $\text{VO}_2$ -coated microstring, which closely matched the obtained experimental observations. We demonstrate that localized temperature difference across the microstring changes significantly because of the Joule heating. This change in temperature thus changes the resonance frequency of the micro-string. The MIT behavior of  $\text{VO}_2$  can be greatly tuned by controlling the tensile stress of the film. Larger tensile stress shifts the MIT towards higher temperature as well as higher  $E_c$ , whereas larger compressive stress opposes both. Therefore to achieve MIT at lower temperature titanium dioxide ( $\text{TiO}_2$ ) was used as a buffer layer at the interface, which facilitates compressive stress during the growth of  $\text{VO}_2$ , leading  $T_c$  to be lowered.<sup>44</sup>

## 2. Experimental details

Nanomechanical devices (microstrings) were fabricated using a nanofabrication facility. First, boron-doped p-type (100) Si wafers (dia ~ 4”) were thermally oxidized *via* wet oxidation in a tube furnace (Tystar) of 1.5  $\mu\text{m}$  thickness at 1050 °C, followed by deposition of 200 nm thick stoichiometric silicon nitride ( $\text{SiN}_x$ ) on top by low-pressure chemical vapor deposition (LPCVD). The film stress was found to be 1.2 GPa measured by a Flexus 2320 stress measurement tool. The wafers were diced into 12.5 mm × 12.5 mm square-shaped coupons. The wafers are called  $\text{SiN}_x/\text{SiO}_2/\text{Si}$ . The wafers were cleaned in piranha solution followed by cleaning in acetone, IPA and water before depositing  $\text{TiO}_2$  and  $\text{VO}_2$  using the pulsed laser deposition (PLD) technique (as shown in Fig. S1 ESI†). Both  $\text{VO}_2$  and  $\text{TiO}_2$  were deposited onto  $\text{SiN}_x/\text{SiO}_2/\text{Si}$  wafers by (PLD) from vanadium (99.9% purity, American Elements) and titanium metal (99.9% purity, Kurt J Lesker) targets in an oxygen environment. A KrF ( $\lambda = 248$  nm) excimer laser (Coherent, GmbH) was directed at the rotating target with a laser fluence of 2.6  $\text{J cm}^{-2}$  and a repetition rate of 10 Hz. The substrate, maintained at 600 °C for the duration of the deposition, was placed directly opposite to the target, 31 mm apart. Oxygen pressure was maintained at 10 mTorr for  $\text{TiO}_2$  and 50 mTorr for  $\text{VO}_2$  deposition. Initially,  $\text{TiO}_2$  was deposited for 15 min followed by 30 min annealing time before depositing  $\text{VO}_2$  for 15 min. Parameters for the  $\text{VO}_2$  deposition were fully optimized in our previous work.<sup>45</sup> After deposition, the phase and crystallinity were determined using the Rigaku XRD Ultima IV instrument and the surface morphology was studied by Bruker Dimension Icon atomic force microscopy (AFM). To validate



the presence of  $\text{TiO}_2$  and  $\text{VO}_2$  and measure their thicknesses, transmission electron microscopy (TEM) was performed using a T20 microscope (ThermoFisher TecnaiTM T20) equipped with a LaB<sub>6</sub> filament operated at 200 kV. TEM foils of thickness less than 100 nm were prepared using focused ion beam (FIB) machining, followed by the liftoff. The Raman characteristics of  $\text{TiO}_2$  and  $\text{VO}_2$  were studied using a Raman Spectrometer (model WITec alpha300R). The fabrication of  $\text{VO}_2/\text{TiO}_2$  microstring was carried out by various microfabrication processes, as shown in Fig. 1(a)–(i), which have been discussed in our recent work.<sup>46</sup> Here, we would like to emphasize that for maximum yield of nanomechanical devices, the greatest challenges lie in the release of the micro-string by etching the sacrificial  $\text{SiO}_2$  layer while protecting the  $\text{VO}_2/\text{TiO}_2/\text{SiN}_x$  layer above it. For this, the efficient process was to etch  $\text{VO}_2$ ,  $\text{TiO}_2$  and  $\text{SiN}_x$  *via* reactive ion etching (RIE) while protecting the device with a Cr hard mask. Here again, the optimum choice of etchant gas and etching rate was necessary to avoid undercut and excess material removal, which was optimized by us in our earlier works.<sup>46</sup> The VHF etchant was used to remove the sacrificial layer and release the micro-string as it prevents stiction issues which are commonly observed while using BOE as an etchant, thus maximising the yield, which was found to be more than 90%.

All the microstrings were anchored to the contact pads of  $3\text{ mm} \times 3\text{ mm}$  dimensions coated with Au (80 nm)/Ti (20 nm) by E-beam evaporation. The dimension of the fabricated micro-string resonator used in this study was  $400\text{ }\mu\text{m}$  ( $L$ )  $\times$   $3\text{ }\mu\text{m}$  ( $W$ )  $\times$   $240\text{ nm}$  ( $t$ ) as shown in the SEM image (Fig. 1(j)).

Furthermore, to investigate the electrical and mechanical behavior of microstring resonators, two independent measurements were carried out to probe MIT of  $\text{VO}_2$ . In one case electrical resistance and  $I$ - $V$  characteristics were performed with the function of temperature while in the other case, the resonance frequency of the device was measured again with the function of temperature. The former was performed by mounting the device on a probe station (Signatone) using a Keithley 2636 source meter by varying the temperature from  $5\text{ }^\circ\text{C}$  to  $100\text{ }^\circ\text{C}$  at an interval of  $2\text{ }^\circ\text{C}$ , equilibrating for 5 min in both the heating and cooling cycles. The latter, *i.e.* the measurement of resonance frequency, was carried out inside a vacuum chamber (at a pressure of 0.01 mTorr) using a laser Doppler vibrometer (LDV) (Polytech MSA500), as shown in Fig. 2(a) and (b). Furthermore, to study the  $E$ -field-dependent mechanical frequency of microstring, the experimental setup was modified using an in-house built additional attachment, where  $E$ -field was applied using electrical probes onto the contact pads. The two-probe setup was used to apply electric voltage across  $\text{VO}_2$  strings. Two aluminum sheets were bent in bracketed shapes and screwed on a PET (insulating) surface, which was screwed on a micro-manipulator. This would allow one to move the stage laterally and vertically. Spring-loaded pogo pins were glued at the unscrewed side of the brackets in such a way that they were fully compressed when they contacted the sample surface. Electrical connections were made *via* male–female adapters attached to the pogo pin-bracket set up *via* electrical feed, as shown in Fig. 2(c) and (d). The entire attachment along with the microstring device was kept inside the

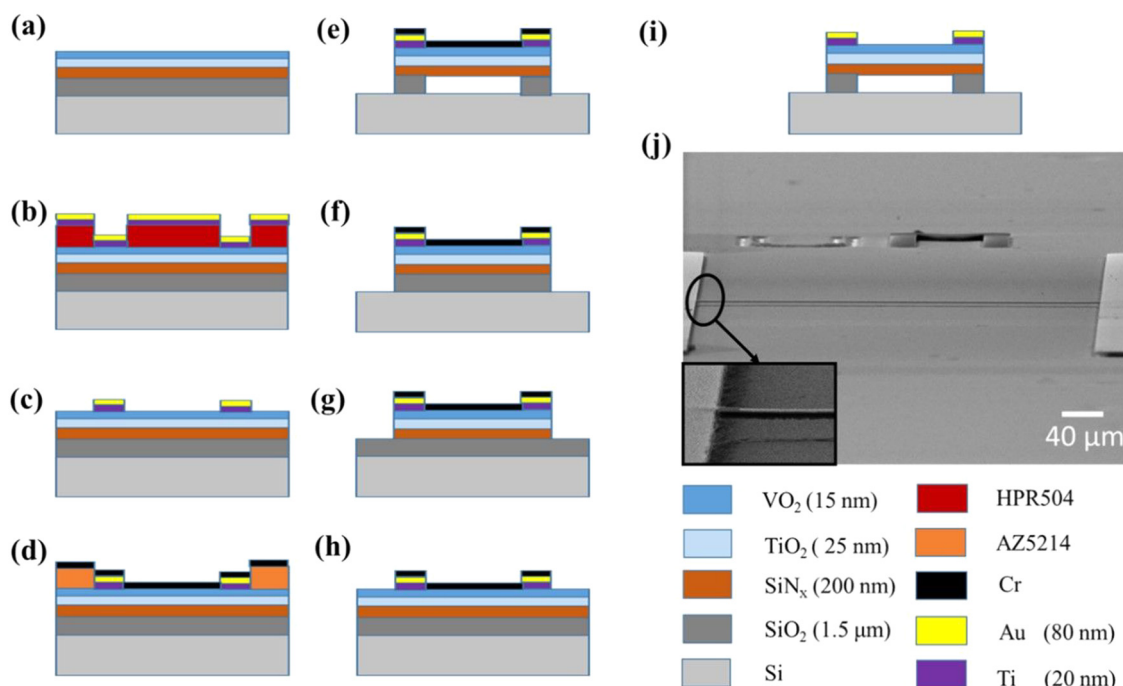


**Fig. 1** Process flow to fabricate suspended nanomechanical resonator. (a) PLD-grown  $\text{VO}_2/\text{TiO}_2$  on the starting substrate ( $\text{SiN}_x/\text{SiO}_2/\text{Si}$ ). (b) HPR504 photoresist spin-coated to a thickness of about  $1.3\text{ }\mu\text{m}$ , followed by patterning of contact pads by lithography and deposition of Au/Ti (80/20 nm) *via* sputtering. (c) Removal of resist in acetone to obtain contact pads. (d) Photoresist coating of AZ5214 by image reversal and lithography to deposit the Cr mask. (e) Stripping away photoresist by acetone through sonication. (f) RIE etching of  $\text{VO}_2$ ,  $\text{TiO}_2$  and  $\text{SiN}_x$  through  $\text{CHF}_3$ ,  $\text{CF}_4$ , and  $\text{O}_2$ -based plasma. (g) Vertical removal  $\text{SiO}_2$ . (h) Release of string by VHF etching of  $\text{SiO}_2$ . (i) Removal of Cr mask by ICP to obtain the final microstring. (j) SEM image of the suspended nanomechanical device (micro-string).

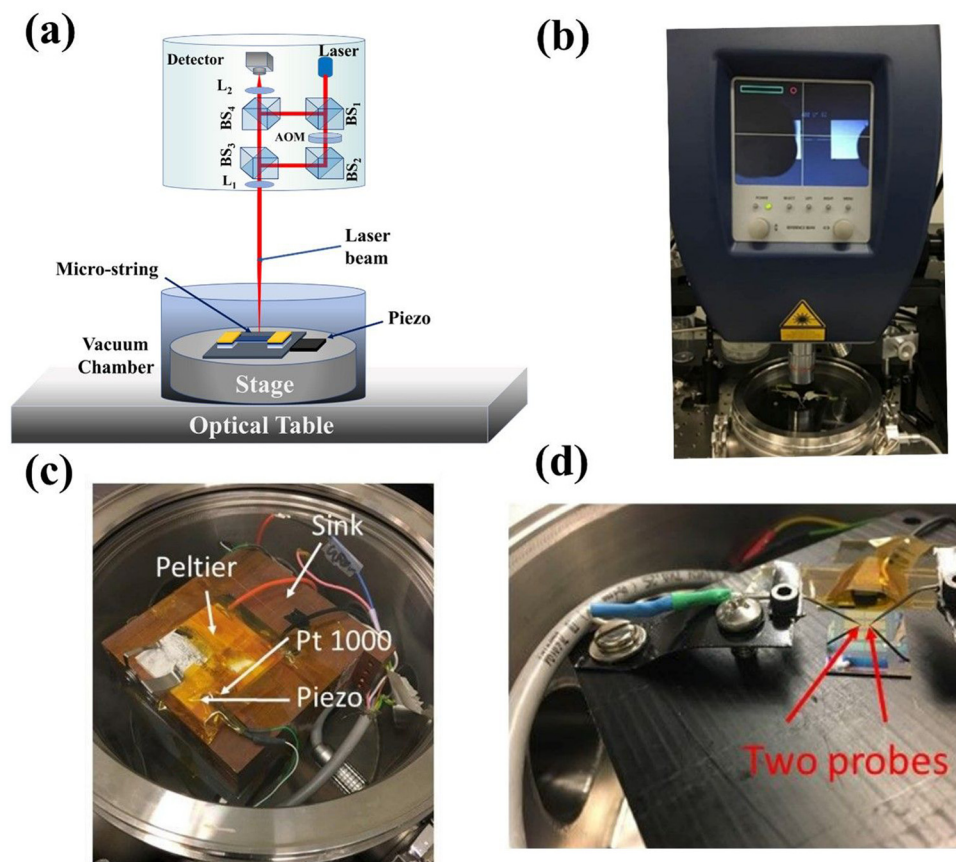


Fig. 2 (a) Schematic of LDV, (b) image of the LDV instrument, (c) integrated vacuum setup for electrical measurements, (d) zoomed electrical setup showing probe connections with contact pads of microstrings.

vacuum chamber wherein the device was rested on a peltier-driven heating stage. A piezo buzzer was mounted beside the device to facilitate the forced vibration to the microstring resonator.

During the measurement, the temperature of the heater was swept from 20 °C to 100 °C at an interval of 2 °C equilibrating for 5 min in both the heating and cooling cycle. The controlled *E*-field was supplied *via* a BK Precision 9183 DC power supply with a computer-controlled software program. Dynamic mechanical response (frequency and amplitude) of the microstrings was recorded *via* LDV, at a pressure of  $2.5 \times 10^{-5}$  mbar as a function of the input electric field across the microstring *via* Au/Ti contact pads. A red laser (633 nm), built-in with LDV, with a minimum laser intensity of 22  $\mu$ W was used to record the Doppler shift. The input voltage was ramped at 1 V min<sup>-1</sup> (*E*-field  $\sim 2.5$  V mm<sup>-1</sup> min<sup>-1</sup>) using a DC power supply. Further voltage pulses were toggled between 0 to +15 V, which corresponded to 0 and 37.5 V mm<sup>-1</sup> *E*-field across the microstring, to observe the mechanical response of the strings below and above the E-MIT.

### 3. Results and discussion

#### 3.1 Experimental results

The structural characterizations of the prepared films before fabricating the device were carried out using XRD, which shows

the formation of a polycrystalline VO<sub>2</sub> (M1) phase along with a TiO<sub>2</sub> rutile phase, as depicted in Fig. 3(a). Further identification of the TiO<sub>2</sub> rutile phase and VO<sub>2</sub> monoclinic phase was confirmed *via* Raman spectroscopy. Raman spectrum of the TiO<sub>2</sub> film revealed its characteristic modes at 143 cm<sup>-1</sup>, 235 cm<sup>-1</sup>, 446 cm<sup>-1</sup> and 611 cm<sup>-1</sup> as shown in Fig. 3(b). After the deposition of VO<sub>2</sub> on TiO<sub>2</sub>, the Raman spectra of TiO<sub>2</sub>/VO<sub>2</sub> showed the presence of the TiO<sub>2</sub>-R phase, which overlaps with the monoclinic phase of VO<sub>2</sub>. This overlap is primarily attributed to the stretching and bending of V-O-V with peaks observed at 138 cm<sup>-1</sup>, 193 cm<sup>-1</sup>, 223 cm<sup>-1</sup>, 261 cm<sup>-1</sup>, 308 cm<sup>-1</sup>, 339 cm<sup>-1</sup>, 387 cm<sup>-1</sup>, 442 cm<sup>-1</sup>, and a characteristic peak at 613 cm<sup>-1</sup>, which has been reported in several articles,<sup>47</sup> as shown in Fig. 3(b)-green spectra. Further temperature-dependent Raman study was performed to verify the presence of a monoclinic phase of the VO<sub>2</sub>. As temperature increases beyond the critical temperature (*T<sub>c</sub>*), VO<sub>2</sub> transforms from its monoclinic phase to its rutile phase and therefore all the characteristic vibrational modes associated with the VO<sub>2</sub> monoclinic phase are suppressed, as shown in Fig. 3(c). Transformation of VO<sub>2</sub> from the monoclinic phase to the tetragonal phase induces tensile stress between the layers of VO<sub>2</sub> and TiO<sub>2</sub> due to the lattice mismatch<sup>19</sup> and therefore there is a mode shift in the characteristic peaks (143 cm<sup>-1</sup> and 611 cm<sup>-1</sup>) of the TiO<sub>2</sub> with 4.6 cm<sup>-1</sup> and 6.34 cm<sup>-1</sup>, respectively, which is seen in

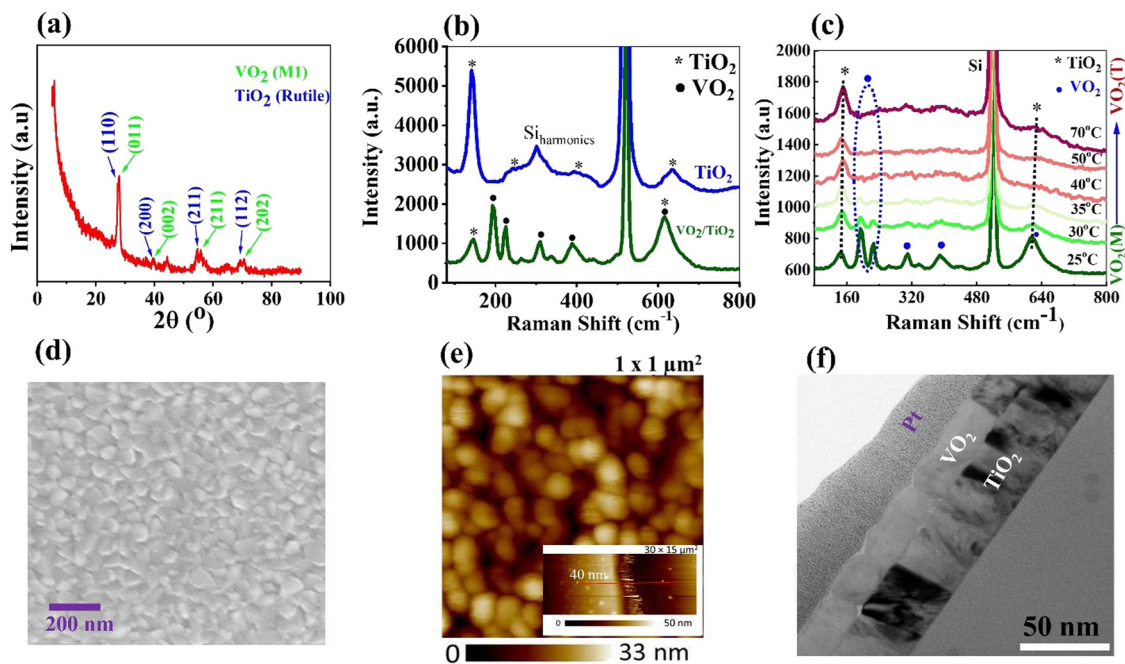


**Fig. 3** (a) XRD of the VO<sub>2</sub> and TiO<sub>2</sub> films over microstring, (b) Raman peaks after TiO<sub>2</sub> deposition and after VO<sub>2</sub>/TiO<sub>2</sub> deposition over microstring, (c) temperature-dependent Raman spectra of VO<sub>2</sub>/TiO<sub>2</sub> String from 25 °C to 70 °C, (d) surface morphology of the top-surface (VO<sub>2</sub> deposited) and (e) AFM image of VO<sub>2</sub>/TiO<sub>2</sub> deposited film with thickness of VO<sub>2</sub>/TiO<sub>2</sub> grown film depicted in inset, (f) TEM image of the VO<sub>2</sub>/TiO<sub>2</sub>/SiN<sub>x</sub> film.

the Raman spectrum beyond the critical temperature, as shown in Fig. 3(c). The shift in the Raman characteristic modes of the TiO<sub>2</sub> is tabulated in Table 1.

Furthermore, the surface morphology after the VO<sub>2</sub> deposition was characterized by scanning electron microscopy (FESEM) and atomic force microscopy (AFM) as shown in Fig. 3(d) and (e). The surface roughness of the VO<sub>2</sub> film was found to be around 4 nm and the morphology was found to be globular in nature, as shown in Fig. 3(e). The total thickness of the film was found to be 40 nm in which TiO<sub>2</sub> and VO<sub>2</sub> were 25 nm and 15 nm each, respectively, (Fig. 3(e) inset). The thickness of the individual films (TiO<sub>2</sub> and VO<sub>2</sub>) was further verified by Transmission electron microscopy (TEM), as shown in Fig. 3(f).

Once the primary characterization was performed, electrical measurements were collected on the fabricated microstring resonator, and it was observed that the electrical resistance of VO<sub>2</sub>-coated microstring reduces more than two orders of magnitude from its original value with the function of temperature when heated from 5 °C to 100 °C and recovers to the initial

value in the cooling cycle with minimal hysteresis of 2 °C, as shown in Fig. 4(a). This large change in electrical resistance is due to the MIT of VO<sub>2</sub>, which occurs between 30 °C to 60 °C because of the structural transformation from the monoclinic (M1) to tetragonal (R) phase, which involves processes such as (Pierels-like) or electron–electron correlation (Mott-like) or both.<sup>48–50</sup> This transition in electrical resistance predominantly occurs in three stages, as depicted in Fig. 4(a). Stage I is the semiconducting (or insulating phase), stage II is the intermediate phase and stage III is the metallic phase.

The width of the hysteresis depends on the poly-crystalline nature of the VO<sub>2</sub> film. Furthermore, it was also noticed in Fig. 4(b), that under bidirectional *I*–*V* sweep, the MIT occurred in the same device at an *E*-field of 27.5 V mm<sup>−1</sup> at 30 °C. MIT under an electric field is often called electric field-dependent MIT (E-MIT). The magnitude of the electric field, to trigger MIT, reduces with increasing temperature. This is because the activation energy required for the transition under an electric field reduces as the device temperature increases.<sup>18</sup> Increment in the temperature of the device on the application of a certain

**Table 1** Observed vibrational Raman modes of TiO<sub>2</sub> with temperature and interface

Temperature (°C)	Raman mode (143 cm <sup>−1</sup> )	Mode shift (Δω)	Raman mode (611 cm <sup>−1</sup> )	Shift (Δω)	Phase
25	145.6	2.6	615.86	4.86	Due to the initial interface of Si <sub>3</sub> N <sub>4</sub> and VO <sub>2</sub> /TiO <sub>2</sub>
30 ← <i>T</i> <sub>c</sub>	147.6	4.6	617.34	6.34	Stage-1 monoclinic
35	150.34	7.34	620.34	9.34	Stage-2 intermediate phase
					Increment in tensile stress due to phase transformation of VO <sub>2</sub> from monoclinic to Rutile.
40	150.34	7.34	620.34	9.34	Stage-3 rutile phase
50	150.34	7.34	620.34	9.34	
70	150.34	5.34	620.34	9.34	



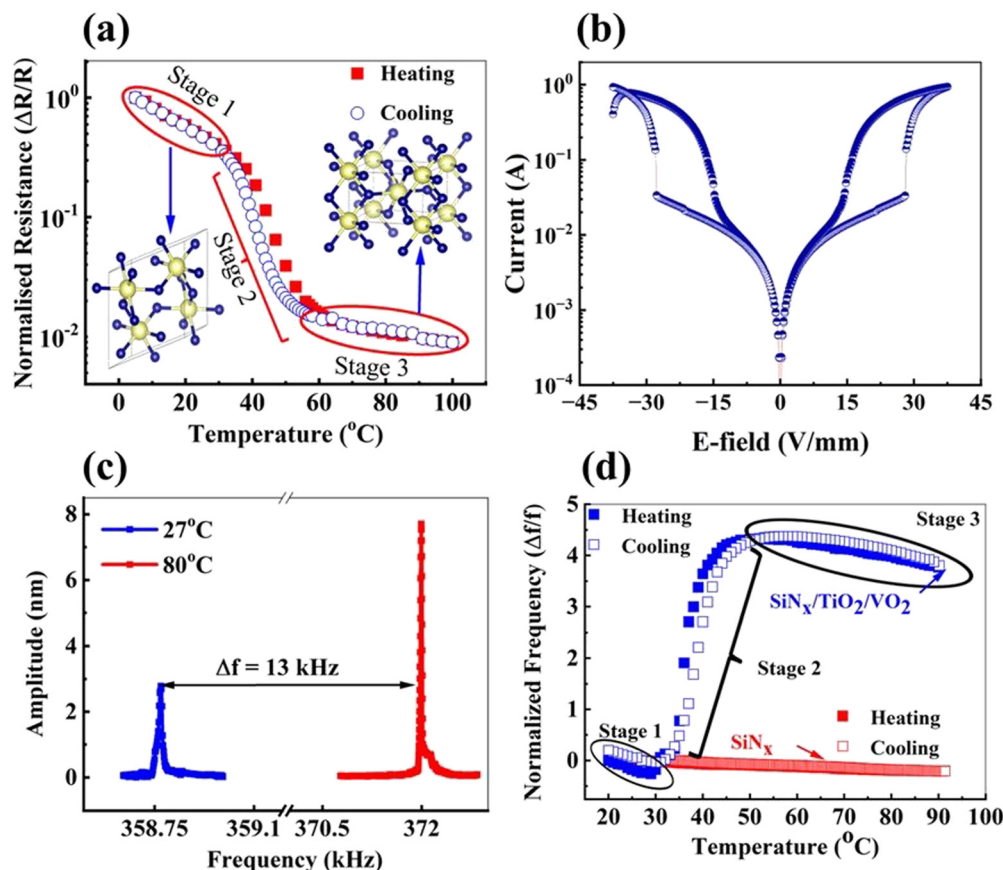


Fig. 4 (a) Resistance changes of VO<sub>2</sub> microstring as a function of temperature. (b) Current flow in VO<sub>2</sub> microstring when an electric-field sweep is performed across it showing E-MIT at room temperature (30 °C). (c) Amplitude response and frequency response at room temperature and high temperature (d) normalized frequency change as a function of temperature of VO<sub>2</sub>-coated and bare (SiN<sub>x</sub>) microstrings.

voltage across the terminal follows eqn (1)<sup>51</sup>

$$T = T_0 + \frac{V^2}{kR} \quad (1)$$

Here,  $T_0$ ,  $k$ ,  $V$  and  $R$ , are the ambient temperature, and thermal parameters (stiffness) that include heat capacities and thermal expansion coefficient, voltage applied across micro-string and resistance of micro-string, respectively. The overall temperature of the device and applied  $E$ -field plays a crucial role in the phase transition of VO<sub>2</sub>.<sup>25,52</sup> Due to the applied  $E$ -field, carrier concentration starts increasing, subsequently after critical  $E$ -field ( $E_c$ ), a sudden increase in the carrier concentration occurs, which further accelerates the carriers under  $E$ -field leading to joule heating and subsequently increase in the temperature, resulting in sudden increment of the current in the device, as shown in Fig. 4(b).<sup>25,51</sup> Furthermore, an investigation of the mechanical response of the nanomechanical resonator was carried out using the laser Doppler vibrometer (LDV), and the data are shown in Fig. 4(c) and (d). The first order resonance frequency ( $f_r$ ) (fundamental mode) of the VO<sub>2</sub>/TiO<sub>2</sub> deposited nanomechanical resonator was measured at 358.7 kHz at room temperature 27 °C with a quality factor ( $Q$ -factor) of 21,876. At a higher temperature of around 80 °C the  $f_r$  of VO<sub>2</sub>/TiO<sub>2</sub>-coated microstrings increased by 3.7% from

358.7 kHz to 372 kHz, as shown in Fig. 4(c) with the reduction in  $Q$ -factor, which was found to be 13 361. For a detailed analysis of the thermo-mechanical behaviour of the nanomechanical resonator, the variation of the normalized resonance frequency of the device as a function of temperature was examined and it was observed that for an uncoated resonator, the resonance frequency change showed a gradual decrease as expected because of the reduction in elastic modulus (as shown in Fig. 4(d)). However, for the VO<sub>2</sub>/TiO<sub>2</sub>-coated nanomechanical resonator, the  $f_r$  decreases initially till 30 °C (can be considered as stage I) and then steeply increase up to around 50 °C (stage II), followed by gradual decrement beyond 50 °C (stage III), as depicted in Fig. 4(d). The observed phenomenon in Fig. 4(d) of the microstring resonator can be explained by the following expression mentioned in eqn (2).<sup>53</sup>

$$f_i = \frac{i^2 \pi}{2l^2} \sqrt{\frac{EI}{\rho A}} \sqrt{1 + \frac{Sl^2}{i^2 EI \pi^2}} \quad (2)$$

where  $i$ ,  $E$ ,  $\rho$ ,  $S$ ,  $A$ ,  $I$  and  $l$  are the mode number of resonance frequency, elastic modulus, volume density, tensile stress, area, area moment of inertia and length of the microstring resonator, respectively. In general, the elastic modulus of any material decreases with increasing temperature,<sup>54</sup> which is given by the

fundamental eqn (3),

$$f = \frac{1}{2\pi} \sqrt{\frac{k}{m}} \quad (3)$$

where  $k$  and  $m$  are the stiffness and mass of the suspended microstring; there is a gradual decrease in the resonance frequency as was observed for the uncoated microstring resonator. For VO<sub>2</sub>, it has been reported<sup>55</sup> that elastic modulus increases steeply at a temperature corresponding to the structural phase transition (SPT) region of VO<sub>2</sub>. At the transition temperature range of VO<sub>2</sub>, there is an increase in tensile stress due to lattice compression taking place in VO<sub>2</sub> because of its transformations from the monoclinic to the tetragonal phase,<sup>42</sup> this fact is also noticed in the Raman spectra of the VO<sub>2</sub>/TiO<sub>2</sub> layers where vibrational modes shift as VO<sub>2</sub> transforms from the monoclinic phase to the rutile phase. Therefore, due to the increase in the tensile stress ( $S$ ) and elastic modulus of VO<sub>2</sub> in the transition temperature range, a sharp rise in its resonance frequency of 3.7% (stage II) is observed, which can also be evident from eqn (2). However, in the region below and above the transition range (stage I and stage III), there is no structural transformation happening (VO<sub>2</sub> is in monoclinic and tetragonal in stage I and stage III, respectively) and the dynamic behaviour is completely controlled by the change in elastic modulus of VO<sub>2</sub> with temperature, thus resulting in gradual decrement of resonance frequency in these two regions. As depicted in Fig. 4, the VO<sub>2</sub>/TiO<sub>2</sub> coated resonator shows unusual behaviour with the variation in temperature as compared to the uncoated SiN<sub>x</sub>/SiO<sub>2</sub>/Si Microstring, which is solely assigned to the solid-state phase transition regardless of Mott-like or Peierls-like. The two observations, as shown in Fig. 4(b) and (d), indicate that this phase transition can be triggered by an electric field, which can modulate the resonance frequency due to the change in the elastic modulus and the tensile stress. In other words, our hypothesis from the previous experiment is that electrical stimulus can modulate and control the mechanical stress or modulus in multiple directions. With the above motivation, we have demonstrated the modulation in the dynamics of the resonance frequency of

the resonator by controlling the strength of the electric field, which is attributed to the EMIT phenomenon. Hence, to investigate the electro-mechanical response of the VO<sub>2</sub>/TiO<sub>2</sub> microstrings, an electric field was applied across the resonator through pogo-pins attached to contact pads. The resonance behaviour of microstring was studied under an electric field applied in two different ways. In the first case, the  $E$ -field was varied across the microstring in pulsating (on and off) manner, corresponding to which the resonance behaviour of strings was observed by measuring resonance frequency with the function of time. In the second case, the resonance frequency of the micro-strings was measured by varying  $E$ -field in a linear ramping rate. In the first case, when the  $E$ -field was applied in a pulsating manner, the  $f_r$  of the resonator dropped by 0.5%, from 360.4 kHz to 358.6 kHz. This frequency remained stable at 358.6 kHz until the  $E$ -field was turned off, at which point it returned to its original value of 360.4 kHz, as shown in Fig. 5(a). However, when the higher  $E$ -field (*i.e.* 25 V mm<sup>-1</sup>) was applied to the resonator in a similar pulsated manner, the resonance behaviour of the microstring just flipped and the corresponding resonance frequency of the resonator increased by 2.5% from 360.4 ± 0.3 kHz to 368.4 ± 0.3 kHz at the on state and dropped to its initial value *i.e.* 360.4 ± 0.3 kHz at the off state as depicted in Fig. 5(b).

To completely understand this resonance behaviour of microstrings due to the toggling of the  $E$ -field, the following approaches have been adopted. The experiment was performed in two different steps. In the first case, the  $E$ -field was toggled (on and off) from 0–15 V mm<sup>-1</sup> to 0–32.5 V mm<sup>-1</sup> in steps of 2.5 V mm<sup>-1</sup>. During this event, it was observed that the magnitude of the drop in resonance frequency (*i.e.*,  $\Delta f_r$ ) of the resonator goes down till the  $E$ -field reaches 20 V mm<sup>-1</sup>. Beyond this value, increments in the resonance frequency of the resonator were observed up to 27.5 V mm<sup>-1</sup>. Further increment in the  $E$ -field (*i.e.* from 27.5 V mm<sup>-1</sup> to 32.5 V mm<sup>-1</sup>), again resulted in the decrement of  $\Delta f_r$ , as shown in Fig. 6(a). At higher  $E$ -field ( $\geq 20$  V mm<sup>-1</sup>), as anticipated from the previous observation shown in Fig. 4(d), due to the localized heating of the microstring, the temperature reaches the range of phase

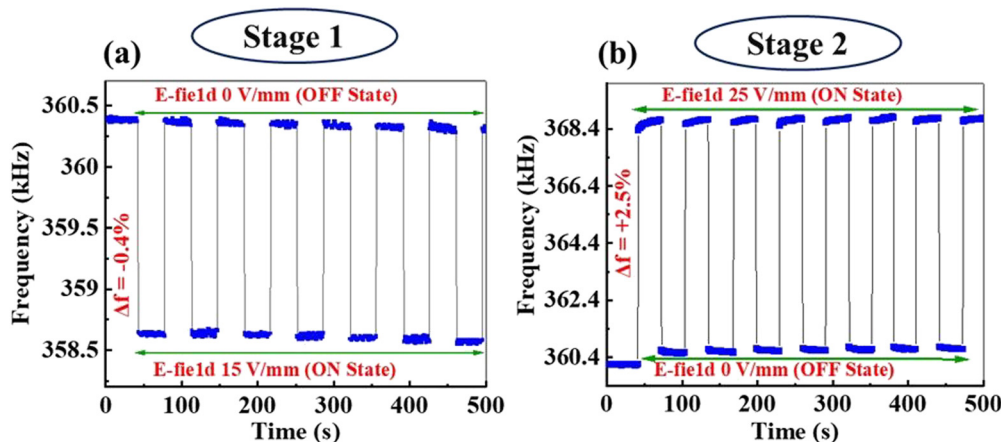


Fig. 5 Mechanical frequency modulation of the VO<sub>2</sub>/TiO<sub>2</sub> microstring as a function of time (a) at 15 V mm<sup>-1</sup> and (b) at 25 V mm<sup>-1</sup> pulsating  $E$ -field.



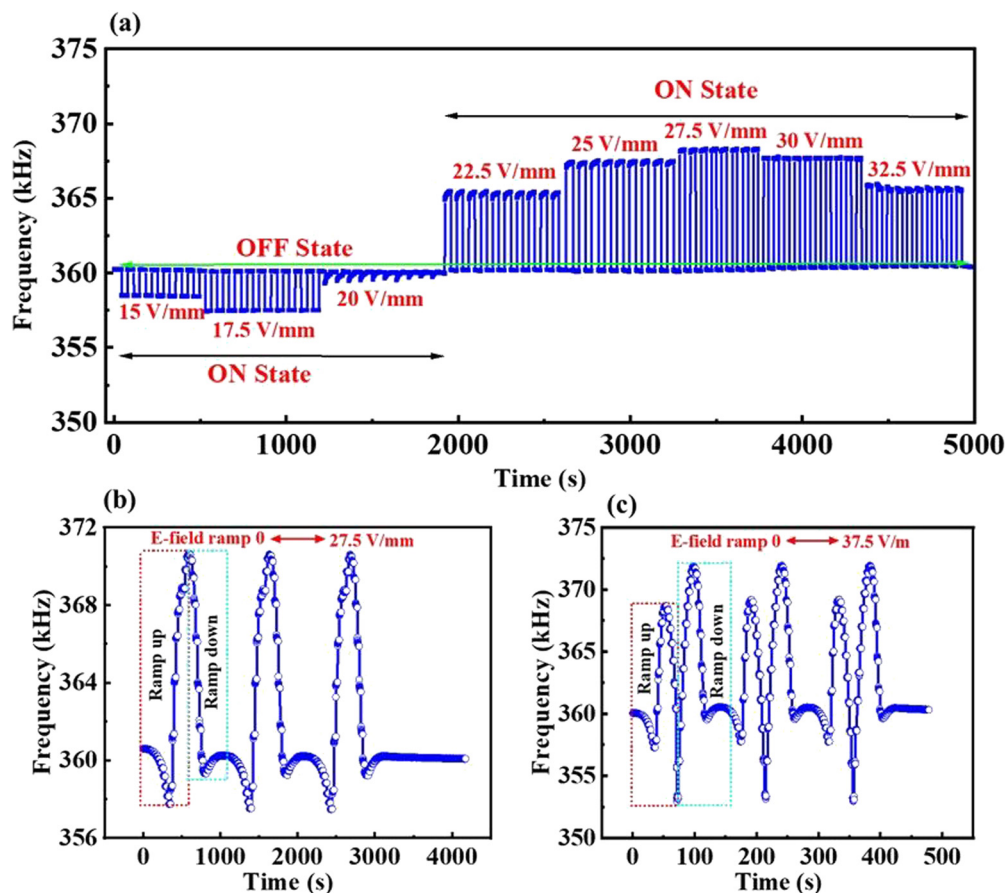


Fig. 6 (a) Frequency response of the VO<sub>2</sub> microstringing as a function of pulsating  $E$ -field from 15 V mm<sup>-1</sup> to 32.5 V mm<sup>-1</sup>, (b) and (c) frequency responses of suspended VO<sub>2</sub> microstringing as a result of ramping  $E$ -field from 0–27.5 V mm<sup>-1</sup> and 0–37.5 V mm<sup>-1</sup>.

transition temperature, which increases the elastic modulus and tensile stress of the resonator (as observed in stage-2 of Fig. 4(d)), resulting in a sharp increase in its resonance frequency. At a very high  $E$ -field (third stage,  $\geq 27.5$  V mm<sup>-1</sup>), once again the stiffness of VO<sub>2</sub>/TiO<sub>2</sub> microstrings reduces and thus its frequency decreases. The switching speed (response time) of the device between the on and off states is very fast as the structural phase transition of VO<sub>2</sub> is believed to be ultrafast as reported in several studies.<sup>56,57</sup> Measuring such a fast response time is limited by the acquisition time of the measuring instrument. Therefore, we were not able to measure and quantify the exact response time of the mechanical frequency response of the microstring resonator. However, in our case, we believe that the response time of the VO<sub>2</sub>-coated resonator is majorly dependent upon the mechanical resonance frequency<sup>58</sup> and the heat conductivity.<sup>59</sup> The micro-string with a higher resonance frequency may possibly have a faster response time. In that case, one needs to play with the geometry of the string (length, width, and thickness) to increase the resonance frequency. Furthermore, heat-conducting and storing parameters such as thermal conductivity and specific heat capacity of the VO<sub>2</sub> and the surrounding material decide the rate of the phase transition of VO<sub>2</sub>. It is desirable to have higher thermal conductivity for efficient phase transition and lower specific heat capacity for

faster switching of transition from the insulator to metal and *vice versa*. In addition to this, the lower volume of VO<sub>2</sub> material ensures faster dissipation of heat and hence enhances response time. The resonance behaviour of microstrings at two different linear rampings of the  $E$ -field in two different ranges of (0–27.5 V mm<sup>-1</sup>) and (0–37.5 V mm<sup>-1</sup>) were performed and data are shown in Fig. 6(b) and (c). It was observed that at the linear ramping of applied  $E$ -field from 0 to 27.5 V mm<sup>-1</sup> with a ramping rate of 2.5 V mm<sup>-1</sup> min<sup>-1</sup>, the frequency of VO<sub>2</sub>/TiO<sub>2</sub> microstring resonator first decreases to 358.5 kHz till the  $E$ -field reaches 20 V mm<sup>-1</sup> and subsequently increase to 370.5 kHz till the  $E$ -field reaches 27.5 V mm<sup>-1</sup>. While ramping down the  $E$ -field, the resonance frequency of the resonator drops down to 22.5 V mm<sup>-1</sup> and then rises to the original state of resonance frequency (360.4 kHz) at 0 V mm<sup>-1</sup>. This resonance behaviour of microstrings during the ramping of the  $E$ -field undergoing trough and crest constitutes one cycle and follows the same periodic pattern when repeated ramping of the  $E$ -field was performed as shown in Fig. 6(b).

The periodic pattern in the resonance behaviour of VO<sub>2</sub>/TiO<sub>2</sub> microstrings showed two peaks in one cycle when the  $E$ -field was varied from 0–37.5 V mm<sup>-1</sup>. This phenomenon can be explained from the obtained results of the resonance behaviour of microstrings during the toggling action of  $E$ -field as

described earlier. The first peak is due to the increment of the  $E$ -field from 0 to  $37.5 \text{ V mm}^{-1}$  while the second peak is because of the reduction of the  $E$ -field from  $37.5 \text{ V mm}^{-1}$  to  $0 \text{ V mm}^{-1}$ , as shown in Fig. 6(c). Careful observation delineates the reason for such unusual behaviour. From Fig. 6(a) it is clear that at a higher field than  $27.5 \text{ V mm}^{-1}$  the amplitude of the increment of frequency decreases, hence, when  $E$ -field was applied to the resonator from 0 to  $37.5 \text{ V mm}^{-1}$  it underwent a lowering of its frequency initially followed by a sharp increase in the  $f_r$ . However, while decreasing the field from  $37.5 \text{ V mm}^{-1}$  to 0, it again undergoes critical values of  $E$ -field (*i.e.*  $27.5 \text{ V mm}^{-1}$ ), which shows a further increment in the frequency shift. The periodic pattern in the mechanical resonance frequency of the  $\text{VO}_2$ -coated microstring is different from that of the periodic input  $E$ -field (shown in Fig. 6(c) and (d)). The possible explanation for this behaviour could be that ramping is performed in a continuous manner, which results in a faster rate of heat generation as compared to the rate of heat dissipation. Consequently, the output waveform varies compared to the input. The electromechanical response of the microstring resonator is promising. The immediate application that can be implemented by the obtained results is in the application of switching devices as the graph depicted in Fig. 5(a) and (b) can be modelled as the not gate and buffer gate as shown in Fig. 7(a) and (b), respectively. The micro-string modulated at a lower  $E$ -field or below MIT shows a drop in resonance frequency. If we consider  $0 \text{ V mm}^{-1}$  and  $15 \text{ V mm}^{-1}$  as high and low values, then the resonance frequency corresponding to  $15 \text{ V mm}^{-1}$  is reverse *i.e.*, at lower  $E$ -field higher resonance frequency and at higher  $E$ -field lower frequency is the output from the resonator. Thus, it works like a NOT gate. At a higher  $E$ -field around  $27.5 \text{ V mm}^{-1}$ , the behaviour is just reversed. In this case,  $0 \text{ V mm}^{-1}$  corresponds to lower frequency and higher  $E$ -field relates to higher resonance frequency, thus resembling

the model of a double NOT gate or buffer gate. Similarly, the ramping response of the resonator can be implemented to obtain certain analogue behaviour, as shown in Fig. 7(c) and (d). Apart from this, pattern recognition applications can be modelled depending on the periodic frequency response of the  $\text{VO}_2/\text{TiO}_2$ -coated nanomechanical resonator on the application of the  $E$ -field applied in a periodically linear ramping manner. It is evident from the result that the periodic frequency response of the resonator is unique for two different linear ramping  $E$ -fields depending on the strength of the field. Therefore, one can store periodic frequency patterns corresponding to different ranges of linear ramped  $E$ -field as a reference signal and can compared to the frequency pattern generated from the test device to match the identity.

### 3.2 Simulation results

The simulation studies were carried out using FEM calculations to study and validate the obtained experimental results. The thermo-mechanical response of microstrings obtained using FEM studies is shown in Fig. 8. The simulated and the experimental result matches with good accuracy in the transition temperature region described in our work. However, there is a deviation in the obtained resonance frequency *vs.* the temperature curve in the simulation in comparison to the experimental result. We believe that this could be due to the fact that in reality there are many more factors such as defect and interfacial effects arising between  $\text{TiO}_2$  and  $\text{VO}_2$  that are difficult to incorporate into the simulation. The objective of the simulation was to observe the role of  $\text{TiO}_2$  in lowering the transition temperature range of  $\text{VO}_2$  and this has been accomplished by us. Here, we have designed the nanomechanical resonator as per the dimensions of the fabricated micro-string. The  $\text{VO}_2/\text{TiO}_2$  material was just added above it in the form of a uniformly distributed load (UDL). From the experimental data, combined Young's modulus values of  $\text{VO}_2$ ,  $\text{TiO}_2$  and  $\text{SiN}_x$  were considered at different temperatures ranging from

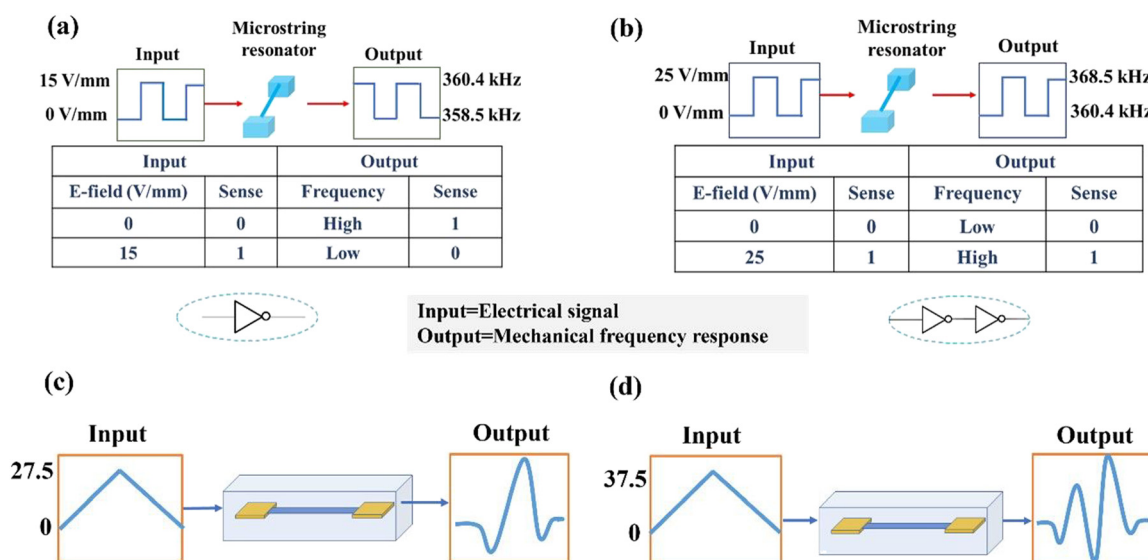


Fig. 7 Schematic sketch and truth table corresponding to (a) NOT gate, (b) buffer gate and frequency response pattern corresponding to the ramping signal from (c) 0 to  $27.5 \text{ V mm}^{-1}$ , (d) 0 to  $37.5 \text{ V mm}^{-1}$ .

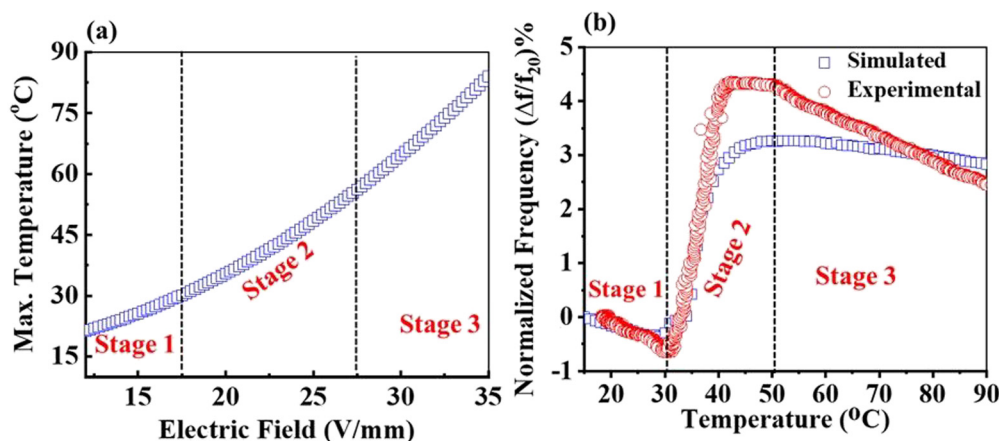


Fig. 8 (a) Maximum temperature across microstringing due to applied electric field, (b) fundamental frequency variation of microstringing as a function of temperature.

(20 to 100 °C). Further details of the entire simulation results are explained in the ESI† (S2 and S3). To understand the  $E$ -field induced MIT of  $\text{VO}_2$ , FEM studies involving localised heating of the  $\text{VO}_2$  microstring on the application of DC-potential, were simulated. In this simulation, only  $\text{VO}_2$  and  $\text{TiO}_2$  layers were considered as  $\text{SiN}_x$  is an insulating material and therefore current will only pass through the  $\text{VO}_2/\text{TiO}_2$  layers. It is clear from the result as shown in Fig. 8(a) that application of a voltage across micro-string induces localised Joule heating effect and thus raise the temperature to an appreciable amount. At higher  $E$ -field or voltage localised temperature goes beyond MIT temperature. However, at lower  $E$ -field, it is well below the MIT temperature range. This result along with the thermo-mechanical simulation explains our experimental findings regarding the  $E$ -field-induced mechanical frequency switching behaviour of the  $\text{VO}_2$ -based microstring resonator.

## 4. Conclusions

In summary, we report the fabrication of a  $\text{VO}_2$ -coated suspended microstring resonator of length 400  $\mu\text{m}$  along with  $\text{TiO}_2$  as an interfacial layer between the  $\text{VO}_2$  and  $\text{SiN}_x$  layers. Structural characterization (XRD and Raman) showed that the deposited films are of polycrystalline nature and form the  $\text{VO}_2$  (M1) phase predominantly, the interfacial  $\text{TiO}_2$  layer forms as a rutile phase, which facilitates a lower stress thereby, reducing the phase transition temperature of  $\text{VO}_2$  from the M1 to R phase. Furthermore, we explored the mechanical modulation of the fabricated nanomechanical resonator by applying an electric field to the terminal points of the resonator and recording its dynamics by measuring the frequency of the device. Our observation was revealed by modulating the DC  $E$ -field, we are able to tune the mechanical frequency of the resonator in both directions (upward and downward) and the magnitude of the  $E$ -field can alter this mechanical modulation from 0.8 to 3.1%. We foresee that the resonance behaviour of  $\text{VO}_2/\text{TiO}_2$  microstrings due to the toggling action of  $E$ -field can be used as different states like what is observed in electronic switches and

hence can be implemented in logic gate applications and consequently in the making of ultra-fast switching devices. Similarly, the periodic pattern in the resonance behaviour of microstrings on the application of different ramping  $E$ -field is unique and can be thought of utilizing this behaviour in the application of pattern recognition with some aid of machine learning algorithm. Therefore, the results obtained on the resonance behaviour of microstrings under two different modes of operation of the  $E$ -field have paved the way for ultrafast switching, logic gates and interesting neuromorphic applications.

## Data availability

The data that support the findings of this study are available within the article and its ESI.†

## Conflicts of interest

There are no conflicts to declare.

## Acknowledgements

AG would also like to thank for SRG 2019/001984 from SERB, DST, FIST grant (SR/FST/ET-I/2020/628) from DST for the establishment of department Raman facility, SERB for the start-up grant, IIT Delhi for MFIRP (MI02442G) and SEED (PLN12/04MS) grant. The authors acknowledge the Department of Materials Science and Engineering (DMSE), Central Research Facility (CRF) and Nanoscale Research Facility (NRF) IIT Delhi and their staff, students and coordinators for helping and allowing to use of various characterization facilities. DB and JKA acknowledge the help from Mr Prashant Sharma from Semiconductor Device Fabrication Group, CSIR-CEERI, Pilani, India to operate the LDV. SAB would like to offer his gratitude to the facilities and staff of nanoFAB at the University of Alberta (U of A), Edmonton, Canada. AG and SAB acknowledge discussions with Prof. Thomas Thundat (Chemical and Biological Engineering SUNY, Buffalo) and for extending his support while he was at CME at



U of A. Authors also offer their gratitude to the group members of the Advanced Electronic Materials and Systems (AEMS) Lab at IIT Delhi. HK and SKM acknowledge the TEM facility at AFMM, IISc Bangalore.

## References

- 1 E. Strelcov, Y. Lilach and A. Kolmakov, *Nano Lett.*, 2009, **9**(6), 2322–2326.
- 2 J. Lu, T. Sagawa, L. Zhang, H. Takagi, D. F. Wang, T. Itoh and R. Maeda, presented at the The 8th Annual IEEE International Conference on Nano/Micro Engineered and Molecular Systems, 2013 (unpublished).
- 3 E. Bayraktar, D. Eroglu, A. T. Ciftlik and H. Kulah, presented at the 2011 IEEE 24th International Conference on Micro Electro Mechanical Systems, 2011 (unpublished).
- 4 D. Shen, J.-H. Park, J. Ajitsaria, S.-Y. Choe, H. C. Wickle and D.-J. Kim, *J. Micromech. Microeng.*, 2008, **18**(5), 055017.
- 5 A. S. Algamili, M. H. M. Khir, J. O. Dennis, A. Y. Ahmed, S. S. Alabsi, S. S. Ba Hashwan and M. M. Junaid, *Nanoscale Res. Lett.*, 2021, **16**(1), 16.
- 6 K. L. Ekinci, *Small*, 2005, **1**(8–9), 786–797.
- 7 B. Xu, J. Zhu, F. Xiao, C. Jiao, Y. Liang, T. Wen, S. Wu, Z. Zhang, L. Lin, S. Pei, H. Jia, Y. Chen, Z. Ren, X. Wei, W. Huang, J. Xia and Z. Wang, *Small*, 2023, **19**(24), 2300631.
- 8 G. E. Fantner, P. D. Odermatt and H. A. Eskandarian, *Springer Handbook of Nanotechnology*, Springer, 2017, pp. 587–616.
- 9 F. C. Hoppensteadt and E. M. Izhikevich, *IEEE Trans. Circuits Syst. I. Fundam. Theory Appl.*, 2001, **48**(2), 133–138.
- 10 H. Yamaguchi and I. Mahboob, *Foundations of Quantum Mechanics in the Light of New Technology*, WORLD SCIENTIFIC, 2009, pp. 295–300.
- 11 S. Zhao, L. Li, C. Hu, B. Li, M. Liu, J. Zhu, T. Zhou, W. Shi and C. Zou, *Adv. Sci.*, 2023, **10**(21), 2300908.
- 12 A. Holsteen, I. S. Kim and L. J. Lauhon, *Nano Lett.*, 2014, **14**(4), 1898–1902.
- 13 M. Javanbakht, S. Mohebbi and H. Attariani, *ACS Appl. Electron. Mater.*, 2023, **5**(6), 3521–3530.
- 14 J. A. Kalb, Q. Guo, X. Zhang, Y. Li, C. Sow and C. V. Thompson, *J. Microelectromech. Syst.*, 2008, **17**(5), 1094–1103.
- 15 Y. Wang, J. Chai, S. Wang, L. Qi, Y. Yang, Y. Xu, H. Tanaka and Y. Wu, *J. Appl. Phys.*, 2015, **117**(6), 064502.
- 16 A. G. Gavriliuk, I. A. Trojan and V. V. Struzhkin, *Phys. Rev. Lett.*, 2012, **109**(8), 086402.
- 17 F. Wrobel, H. Shin, G. E. Sterbinsky, H.-W. Hsiao, J.-M. Zuo, P. Ganesh, J. T. Krogel, A. Benali, P. R. C. Kent, O. Heinonen and A. Bhattacharya, *Phys. Rev. Mater.*, 2019, **3**(11), 115003.
- 18 K. Liu, S. Lee, S. Yang, O. Delaire and J. Wu, *Mater. Today*, 2018, **21**(8), 875–896.
- 19 U. Chitnis, S. Kumar, S. A. Bukhari, C. Soren, R. K. Ghosh and A. Goswami, *Appl. Surf. Sci.*, 2023, **637**, 157916.
- 20 Z. Shao, X. Cao, H. Luo and P. Jin, *NPG Asia Mater.*, 2018, **10**(7), 581–605.
- 21 A. Gupta, R. Aggarwal and J. Narayan, *MRS Online Proc. Libr.*, 2009, **1174**(1), 19–24.
- 22 M. Soltani, M. Chaker, E. Haddad, R. V. Kruzelecky and J. Margot, *Appl. Phys. Lett.*, 2004, **85**(11), 1958–1960.
- 23 M. Rini, Z. Hao, R. W. Schoenlein, C. Giannetti, F. Parmigiani, S. Fourmaux, J. C. Kieffer, A. Fujimori, M. Onoda, S. Wall and A. Cavalleri, *Appl. Phys. Lett.*, 2008, **92**(18), 181904.
- 24 H. Lim, N. Stavrias, B. C. Johnson, R. E. Marvel, R. F. Haglund and J. C. McCallum, *J. Appl. Phys.*, 2014, **115**(9), 093107.
- 25 G. Stefanovich, A. Pergament and D. Stefanovich, *J. Phys.: Condens. Matter*, 2000, **12**(41), 8837–8845.
- 26 B. Viswanath, C. Ko and S. Ramanathan, *Scr. Mater.*, 2011, **64**(6), 490–493.
- 27 Y. Cui, Y. Ke, C. Liu, Z. Chen, N. Wang, L. Zhang, Y. Zhou, S. Wang, Y. Gao and Y. Long, *Joule*, 2018, **2**(9), 1707–1746.
- 28 Q. Cheng, S. Paradis, T. Bui and M. Almasri, *IEEE Sens. J.*, 2011, **11**(1), 167–175.
- 29 L. Pellegrino, N. Manca, T. Kanki, H. Tanaka, M. Biasotti, E. Bellingeri, A. S. Siri and D. Marré, *Adv. Mater.*, 2012, **24**(21), 2929–2934.
- 30 N. Manca, L. Pellegrino, T. Kanki, S. Yamasaki, H. Tanaka, A. S. Siri and D. Marré, *Adv. Mater.*, 2013, **25**(44), 6430–6435.
- 31 R. B. Naik, D. Verma and V. Balakrishnan, *Appl. Phys. Lett.*, 2022, **120**(6), 062101.
- 32 N. Manca, L. Pellegrino, T. Kanki, W. J. Venstra, G. Mattoni, Y. Higuchi, H. Tanaka, A. D. Caviglia and D. Marré, *Adv. Mater.*, 2017, **29**(35), 1701618.
- 33 C. Chen, X. Yi, X. Zhao and B. Xiong, *Sens. Actuators, A*, 2001, **90**(3), 212–214.
- 34 H. Kim, K. Cheung, R. C. Y. Auyeung, D. E. Wilson, K. M. Charipar, A. Piqué and N. A. Charipar, *Sci. Rep.*, 2019, **9**(1), 11329.
- 35 G. Gopalakrishnan, D. Ruzmetov and S. Ramanathan, *J. Mater. Sci.*, 2009, **44**(19), 5345–5353.
- 36 A. Pergament, P. Boriskov, N. Kuldin and A. Velichko, *Phys. Status Solidi B*, 2010, **247**(9), 2213–2217.
- 37 S.-H. Bae, S. Lee, H. Koo, L. Lin, B. H. Jo, C. Park and Z. L. Wang, *Adv. Mater.*, 2013, **25**(36), 5098–5103.
- 38 S. A. Bukhari, A. Goswami, R. McGee, R. Abraham, D. Hume, H. J. Chung and T. Thundat, presented at the 2020 IEEE 33rd International Conference on Micro Electro Mechanical Systems (MEMS), 2020 (unpublished).
- 39 P. Parikh, C. Chakraborty, T. S. Abhilash, S. Sengupta, C. Cheng, J. Wu and M. M. Deshmukh, *Nano Lett.*, 2013, **13**(10), 4685–4689.
- 40 A. Rúa, F. E. Fernández and N. Sepúlveda, *J. Appl. Phys.*, 2010, **107**(7), 074506.
- 41 R. McGee, A. Goswami, R. Abraham, S. Bukhari and T. Thundat, *MRS Adv.*, 2018, **3**(6–7), 359–364.
- 42 S. A. Bukhari, R. McGee, A. Mahdavi, F. Bensebaa, L. Zhou, H.-J. Chung, T. Thundat and A. Goswami, *Adv. Electron. Mater.*, 2022, **8**, 2100819.
- 43 T. Wang, D. Torres, F. E. Fernández, C. Wang and N. Sepúlveda, *Sci. Adv.*, 2017, **3**(4), e1602697.
- 44 J. Li and J. Dho, *J. Cryst. Growth*, 2014, **404**, 84–88.
- 45 R. McGee, A. Goswami, B. Khorshidi, K. McGuire, K. Schofield and T. Thundat, *Acta Mater.*, 2017, **137**, 12–21.

- 46 R. McGee, A. Goswami, S. A. M. Bukhari, L. Zhou, K. Shankar and T. Thundat, *J. Microelectromech. Syst.*, 2019, **28**(5), 766–775.
- 47 M. Yang, Y. Yang, H. Bin, L. Wang, K. Hu, Y. Dong, H. Xu, H. Huang, J. Zhao, H. Chen, L. Song, H. Ju, J. Zhu, J. Bao, X. Li, Y. Gu, T. Yang, X. Gao, Z. Luo and C. Gao, *Sci. Rep.*, 2016, **6**(1), 23119.
- 48 N. F. Mott, *Proc. Phys. Soc., London, Sect. A*, 1949, **62**(7), 416.
- 49 J. B. Goodenough, *J. Solid State Chem.*, 1971, **3**(4), 490–500.
- 50 J. D. Budai, J. Hong, M. E. Manley, E. D. Specht, C. W. Li, J. Z. Tischler, D. L. Abernathy, A. H. Said, B. M. Leu, L. A. Boatner, R. J. McQueeney and O. Delaire, *Nature*, 2014, **515**(7528), 535–539.
- 51 S. Rathi, J.-H. Park, I.-Y. Lee, J. M. Baik, K. S. Yi and G.-H. Kim, *J. Phys. D: Appl. Phys.*, 2014, **47**(29), 295101.
- 52 A. Zimmers, L. Aigouy, M. Mortier, A. Sharoni, S. Wang, K. G. West, J. G. Ramirez and I. K. Schuller, *Phys. Rev. Lett.*, 2013, **110**(5), 056601.
- 53 S. S. Verbridge, J. M. Parpia, R. B. Reichenbach, L. M. Bellan and H. G. Craighead, *J. Appl. Phys.*, 2006, **99**(12), 124304.
- 54 Y. Cai, K. Zhang, Z. Ye, C. Liu, K. Lu and L. Wang, *Sensors*, 2021, **21**(12), 4242.
- 55 N. Sepúlveda, A. Rúa, R. Cabrera and F. Fernández, *Appl. Phys. Lett.*, 2008, **92**(19), 191913.
- 56 A. S. Johnson, D. Perez-Salinas, K. M. Siddiqui, S. Kim, S. Choi, K. Volckaert, P. E. Majchrzak, S. Ulstrup, N. Agarwal, K. Hallman, R. F. Haglund, C. M. Günther, B. Pfau, S. Eisebitt, D. Backes, F. Maccherozzi, A. Fitzpatrick, S. S. Dhesi, P. Gargiani, M. Valvidares, N. Artrith, F. de Groot, H. Choi, D. Jang, A. Katoch, S. Kwon, S. H. Park, H. Kim and S. E. Wall, *Nat. Phys.*, 2023, **19**(2), 215–220.
- 57 K. A. Hallman, K. J. Miller, A. Baydin, S. M. Weiss and R. F. Haglund, *Adv. Opt. Mater.*, 2021, **9**(4), 2001721.
- 58 P. Sadeghi, A. Demir, L. G. Villanueva, H. Kähler and S. Schmid, *Phys. Rev. B*, 2020, **102**(21), 214106.
- 59 Y. Zhou, S. Su, Z. Zhu, D. Hou, H. Zhang and Y. Cao, *J. Appl. Phys.*, 2024, **136**(13), 130901.